Journal of Korean Association of Crystal Growth
Vol. 6, No. 2 (1996) 194-202

Dislocation structure in hot-pressed polycrystalline TiB_2

Kwang Bo Shim, Brian Ralph* and Keun Ho Auh
CMI(Ceramic Materials Research Institute), Hanyang University, Seoul 133-791, Korea
** Department of Materials Technology, Brunel University of West London, U.K.*

고온가압성형된 다결정 TiB_2내에서 전위구조

심광보, Brain Ralph*, 오근호
한양대학교 세라믹소재연구소, 서울, 133-791
** Department of Materials Technology, Brunel University of West London, U.K.*

Abstract Transmission electron microscopy has been used to characterize the dislocation structure in hot-pressed titanium diboride. The thin foil samples were prepared by the conventional ion beam thinning technique and reveal the main features associated with the dislocations; low-angle grain boundaries with dislocation arrays, high-angle grain boundaries with ledges/steps on the boundary planes. The ledges/steps on the grain boundaries were characterized as the origin of defect structures such as dislocation formation or crack propagation near grain boundaries. A fraction of the high angle grain boundaries contained periodic arrays of grain boundary dislocations. The Burger's vectors of the dislocations in the TiB_2 specimens were determined.

요 약 고온가압성형된 다결정상 titanium diboride내에 형성된 전위구조를 투과전자현미경으로 분석하였다. Ion beam thinner를 사용하여 제작한 박편시편은 전위구조에 대한 특징을 드러내 보였다. 이들 특징들은 전위들로 배열된 저각결정입계, ledges나 steps들이 결정입계면에 존재하는 고각결정입계 등이다. 결정입계에서의 ledges나 steps들은 전위형성이나 결정입계 근처에서의 crack전파와 같은 결함구조로서 평가되었고, 고각결정입계는 부분적으로 결정입계전위를 포함하고 있는 것으로 관찰되었다. 또한, 시편의 미세구조에 존재하는 전위들의 Burger's vectors를 결정하였다.

1. Introduction

Titanium diboride(TiB_2) possesses attractive properties such as a high melting point, a low density, a good thermal conductivity, a high hardness and a good electrical conductivity [1] and its wear and corrosion resistance is superior to many other oxide ceramics [2]. This unique and 'unusual' combination of properties makes this material attractive as an engineering ceramic, especially due to its thermo-physical properties and the possibilities it offers of forming cermets and composite ceramics [3].

The bulk properties of monolithic TiB_2 are mainly governed by the sintered density, the average grain size [4] and the secondary phases present [5,6]. In general, many of the properties of crystalline solids are highly dependent on the defect population and various properties are to a greater or lesser extent controlled by the density and distribution of point defects, line defects (dislocations), and planar defects such as grain and phase boundaries and stacking faults [7]. Therefore, the detailed studies were needed on the hot-pressed TiB_2 ceramic materials in a micro-scale ; especially in terms of the dislocation structure present in the microstructure.

Titanium diboride could have a number of possible slip system, resulting from its hexagonal structure [8]. Many researchers have found the slip systems in TiB_2. Mersol and coworkers [9] suggested that two main glide systems are consistent with the Burgers vector : basal glide $\{0001\}$, $\langle 11\bar{2}0\rangle$ and prismatic glide $\{1\bar{1}00\}$, $\langle 11\bar{2}0\rangle$. Nakano and coworkers [10] deduced the slip system from the orientation of slip lines created by micro-hardness indentions in single crystal TiB_2. They concluded that the major slip systems responsible for the microhardness anisotropy were $\{0001\}\cdot\langle 11\bar{2}0\rangle$ at room temperature and $\{10\bar{1}0\}\ \langle\bar{1}2\bar{1}0\rangle$ at high temperatures. Ramberg and Williams [6] found two other slip systems in polycrystalline TiB_2 to be $\{10\bar{1}0\}\cdot[0001]$ and $\{0001\}\cdot\langle 10\bar{1}0\rangle$. Recently, Wang and Arsenault [11] reported that TiB_2 particles in a NiAl matrix possess three different slip directions ; $[0001]$, $\langle 2\bar{1}\bar{1}0\rangle$ and $\langle 2\bar{1}\bar{1}3\rangle$ and suggested that the possible slip planes were (0001), $\langle 10\bar{1}0\rangle$ and $\langle 10\bar{1}1\rangle$.

In this paper, we present the investigation on the dislocation structure of hot-pressed TiB_2 specimen using a JEOL 2000FX transmission electron microscope with an operating voltage of 200 kV. Transmission electron microscopy combined with energy dispersive X-ray spectroscopy and electron diffraction analysis were used to characterize the dislocation structure which play an important role in the mechanism of hardening and brittleness.

2. Experimental method

2.1. The material

The TiB_2 specimen studied was supplied by Boride Ceramic & Composites Ltd. This specimen was produced by hot-pressing at

approximately 2170℃ under a pressure of 30 MPa for 3 hours. The starting powders contained 0.6 wt% of iron as a major metallic impurity as indicated in Table 1. The relative density of this specimen was equal to 97 % of the theoretical (4520 kgm^{-3}). The average grain size measured by the linear intercept method was found to be about 36.5 μm, whilst the average particle size of the starting powder was about 11.0 μm. X-ray diffraction analysis of this specimen revealed only the presence of TiB_2.

2.2. Sample preparation

TiB_2 pellets were sliced to produce the samples having a thickness of 300 μm using a diamond cutting machine. Both sides of the sliced spcimen were ground mechanically with SiC powders, followed by polishing with 6 μm and 1 μm diamond paste until the thickness of the samples were about 80 μm. Then the final polishing was continued using 0.25 μm diamond paste. The as-polished samples were thinned finally using an argan ion beam thinning machine. An incident ion beam angle of 20° and an average voltage of 4 kV was used during thinning. The average thinning rate was 0.4 μm/hour per gun under these conditions.

Table 1
Chemical composition of the starting powder for the TiB_2 sample from Boride Ceramics & Composites Ltd. (wt%)

Ti	B	C	N	O	Fe
67.3	30.1	0.2	0.3	0.5	0.6

3. Results

3.1. Dislocation arrays

The dislocations of these TiB_2 samples were observed mainly in the larger grains and were often concentrated near the edges of the grain. These dislocations were found to form periodic arrays and networks. Figure 1 shows a periodic array of dislocations

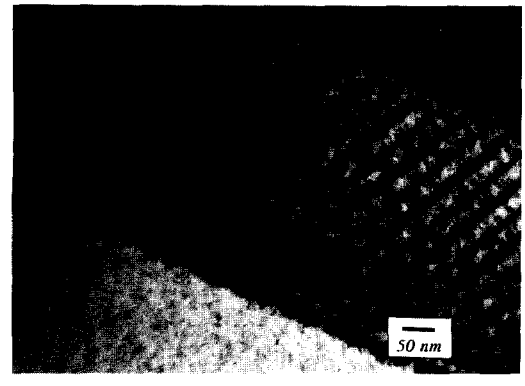

Fig. 1. TEM of periodic arrays of dislocations in TiB_2.

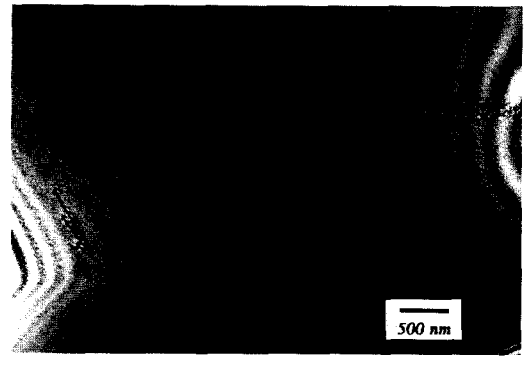

Fig. 2. TEM of subgrain formation observed in a relatively big grain.

across a grain with a spacing in the range of about 20 nm. Figure 2 shows a dislocation network forming a subgrain boundary. These substructures were usually observed in some large grains and the misorientation across this subgrain was found to be less than 1°.

3.2. Dislocation Burgers vectors

The Burgers vector of dislocations in TiB_2 crystals were determined using the well-established '$\mathbf{g}\cdot\mathbf{b}=0$ invisibility criterion', where $\mathbf{g}$ is the reciprocal lattice vector of the operating reflection plane and $\mathbf{b}$ is the Burgers vector of the dislocations. Figures 3 (a)-(h) are bright field micrographs obtained from the different operating reflections in the same region of the sample, showing the visibility of dislocations. The dislocations resloved are selected and labelled A to J. The invisibility of these dislocations are given in Table 2 with different reflecting conditions. For example, the dislocation labelled A is visible in the $(02\bar{2}\bar{1})$ condition but invisible when $(0\bar{2}21)$ is the operating reflection.

The dislocations labelled B, E and F exhibit a similar tendency to become invisible under the same reflection conditions and therefore they must have the same Burgers vectors. They are completely invisible under the reflection condition of $(02\bar{2}\bar{1})$ and $(0\bar{1}11)$. Using the standard (0001) projection for TiB_2 the only low-index directions found along the trace 90° from $(02\bar{2}\bar{1})$ and $(0\bar{1}11)$ poles are $[\bar{2}110]$ and $[2\bar{1}\bar{1}0]$. Therefore, these dislocations have Burgers vectors of $\pm[2\bar{1}\bar{1}0]$. On the other hand, dislocations labelled C, H, I, which are thought to have the same Burgers vectors, are invisible under the $(\bar{1}10\bar{1})$ and $(1\bar{1}01)$ reflecting conditions. The low-index direction traced 90° from these poles on the standard projection

Table 2
The invisibility of dislocations under different diffracting conditions, obtained from tilting the thin foil of a TiB_2 sample (V : clearly visible, I : absolutely invisibel, v : unclearly visible and i : almost invisible)

Goniometer position	Operating reflection planes	Labelled dislocations									
		A	B	C	D	E	F	G	H	I	J
- 10.5°	$(02\bar{2}\bar{1})$	V	I	V	V	I	I	V	V	V	v
- 3.5°	$(0\bar{2}21)$	I	V	V	i	V	V	I	V	V	V
+ 6.0°	$(0\bar{1}11)$	V	I	V	V	I	I	V	V	V	V
+ 14.0°	$(\bar{2}110)$	V	V	V	V	V	V	V	V	V	?
+ 23.5°	$(\bar{1}10\bar{1})$	v	V	I	I	I	I	I	i	I	?
+ 24.5°	$(1\bar{1}01)$	I	V	I	V	V	V	V	i	I	?

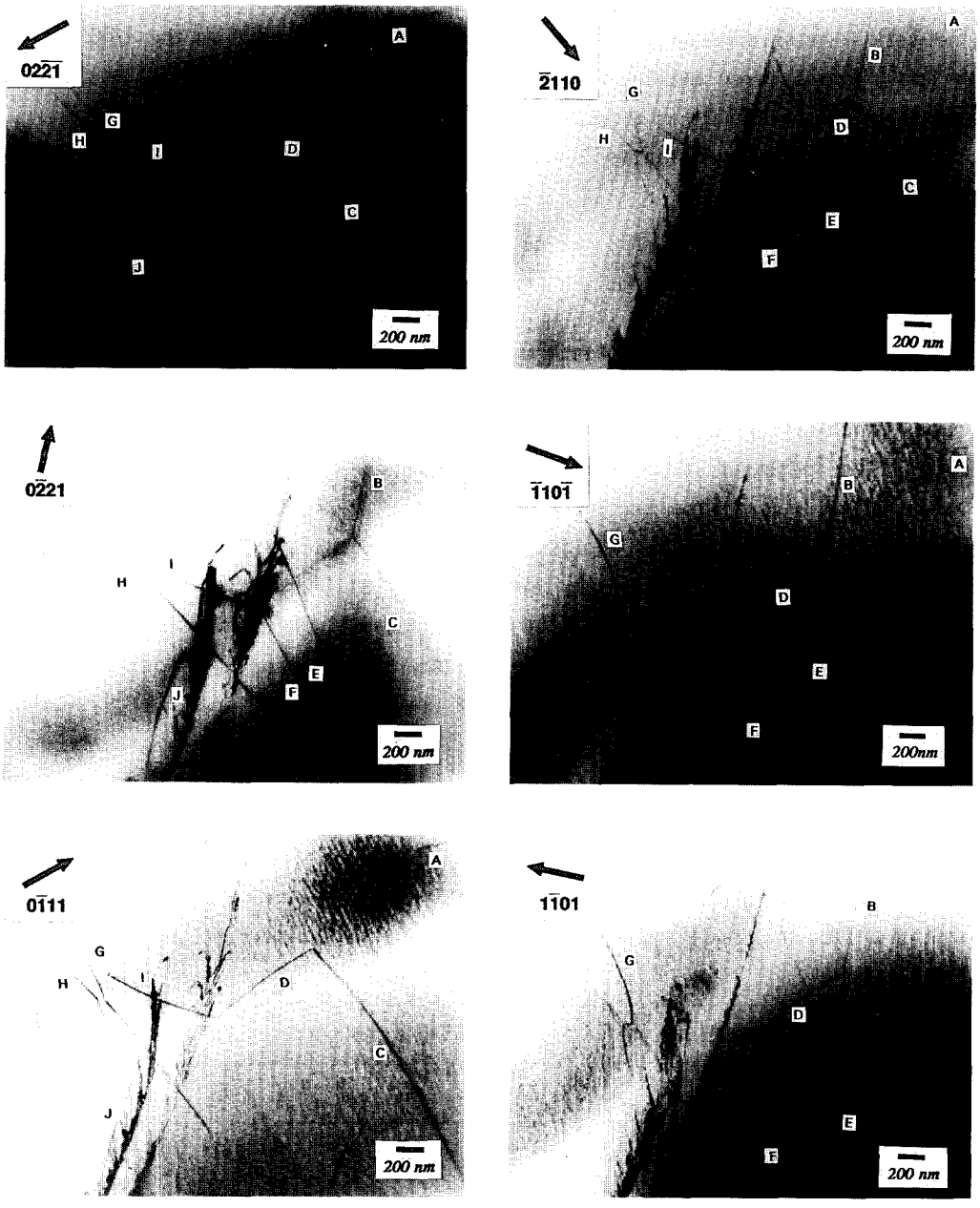

Fig. 3. Changes in contrast of the dislocations depending on the various diffracting conditions obtained from tilting experiments : (a) (02$\bar{2}\bar{1}$), (b) (0$\bar{2}$21), (c) (0$\bar{1}$11), (d) ($\bar{2}$110), (e) ($\bar{1}$10$\bar{1}$) and (f) (1$\bar{1}$01). The letters in each figure are referred to in the text.

was found to be $\pm[11\bar{2}0]$. Therefore, these dislocations have a Burgers vector of $\pm[11\bar{2}0]$. Dislocations with other Burgers vectors were also identified. The dislocation labelled A in Fig. 3 (a) is invisible under the reflection conditions of $(02\bar{2}1)$ and $(1\bar{1}01)$. This dislocation was found to have a Burgers vector of $\pm[\bar{2}203]$.

The dislocations invisible under the high-index reflection condition, such as D and G in Fig. 3 (b), were excluded from Burgers vector determination because it was not possible to get low index reflection conditions. The invisibility of the dislocation labelled J was very difficult to judge because this dislocation was thought to lie underneath the dislocation network.

3.3. *Grain boundary dislocations*

Grain boundaries are usually classified according to the overall geometry which relates the overall orientation change in crossing the boundary plane [7]. When a misorientation (θ) between two grains is smaller than 15° the grain boundary is characterised as of low angle type and its structure may be described by arrays of matrix dislocations which are also called primary intrinsic dislocations [12]. The low-angle subgrain boundaries formed by arrays of these primary dislocations were illustrated in Fig. 2. Similarly, when θ is greater than 15°, the grain boundaries are of high angle type and only secondary dislocation arrays on the grain boundary would be recognizable. Figure 4 is a bright field image of

Fig. 4. TEM of a high angle grain boundary in TiB_2.

a high angle grain boundary in TiB_2. It is seen that one grain is strongly diffracting and therefore gives rise to a thickness fringe pattern which is generally not related to the actual boundary structure.

However, when a high angle grain boundary is near to a coincident site lattice (CSL) orientation its structure exhibits arrays of secondary grain boundary dislocations [7, 13]. Figure 5 shows that a periodic array of dislocations forms in a high angle grain boundary in TiB_2. The dislocation structure is clearly seen in the grain boundary with a spacing of 20-30 nm. Many high angle grain boundaries in TiB_2 thin foils exhibited such periodic grain boundary dislocation structures.

The ledges on the grain boundaries may play a role as donors of dislocations in the grain boundary as illustrated in Fig. 6 (a). Dislocations are clearly seen originating from such ledges. However, if the accommodation of strain stress is not sufficient on

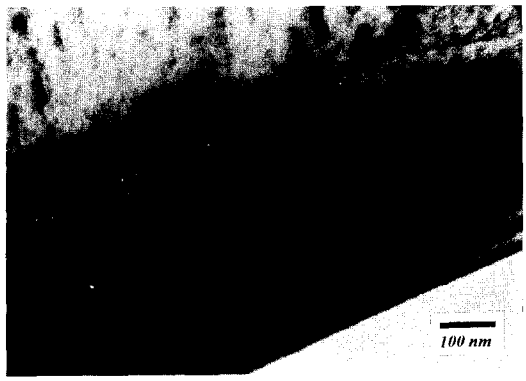

Fig. 5. TEM of high angle grain boundaries with grain boundary dislocations.

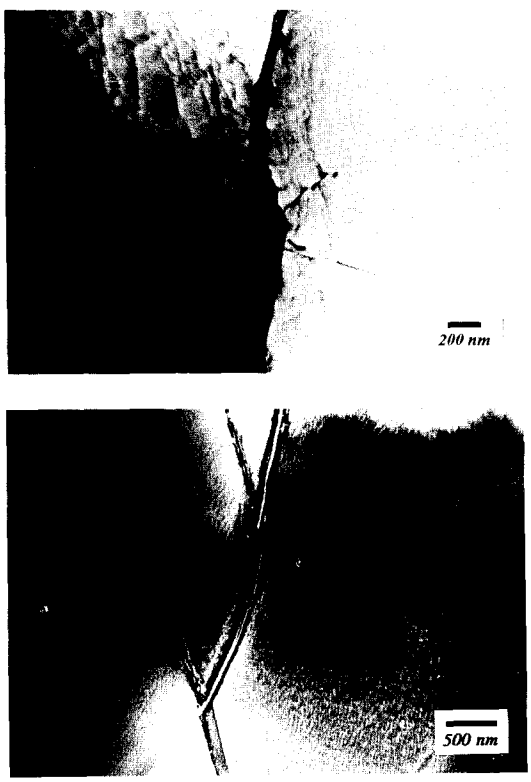

Fig. 6. TEM showing the formation of the ledges/steps on the grain boundary : (a) dislocations originated from ledges and (b) microcracks created from the ledges/steps.

such ledges the propagation of microcracks is possible on such steps from the grain boundary. Figure 6 (b) illustrates this aspect, in particular, when large ledges are non-coherent steps on the boundary plane.

4. Discussion

The dislocations observed in the microstructure of TiB_2 are thought to be originate from the thermal processing, even though it could not be excluded the possibility originated from the initial powder which already contained some lattice defects. The fact that TiB_2 is brittle at room temperature but undergo the metallic-type slip processes above 1000℃ [6] reinforces the possibilty that dislocations could be induced by a variety of way during the thermal processing, especially during the cooling process. Since these dislocations were observed mainly in the large grains and were often concentrated near the edges of the grain, one possible explanation for the dislocation formation is as follows. At the beginning of cooling from the hot-pressing temperature thermal stresses develop due to the anisotropic thermal expansion characteristics of TiB_2 and the internally induced stresses may relax due to dislocation slip, leading to plastic deformation processes.

The presence of well-developed substructures inside grains was characterized by low-angles of misorientation and associated with dislocation arrays or networks. This was good evidence for the presence of the

substructure detected using the electron back-scattered patterns analysis in a scanning electron microscope on TiB_2 [14, 15]. The formation of this substructure was explained by the localised stresses induced during the cooling process as a result of the large anisotropic thermal expansion characteristics of TiB_2. This explanation was reinforced by the observation that these substructures were found preferentially in relatively large grains. These localised stresses may lead to the formation of dislocations in the microstructure which rearrange during slow cooling to lower energy configurations, forming subboundaries. Otherwise, the localised internal stresses should induce spontaneous microcracking since the average grain size of the specimens examined was much larger than the critical grain size ($\gg 15\ \mu m$) [16-18].

On the other hand, Fig. 7 shows an hexagonal stacking fault loop observed in the basal plane of hesagonal TiB_2. Many of the loops lying on {0001} planes take up regular crystallographic forms with their edges parallel to the {1120} direction in the loop plane. These hexagonal stacking faults were not observed in all TiB_2 grains but only a few TiB_2 grains contained this kind of planar imperfection. They were found, far removed from grain boundaries, usually near the centre of a grain, and there were no dislocations observed near them. This could be inferrd to be good evidence to suggest that the grain boundaries and/or dislocations play a role as sinks for vacancies.

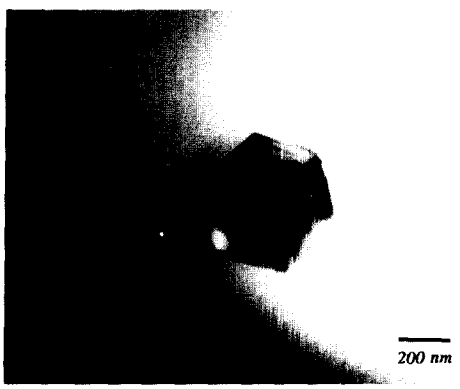

Fig. 7. TEM of a hexagonal stacking fault loop formed in the basal plane of hexagonal TiB_2.

The Burger's vector of the dislocations present in TiB_2 samples were found to be $\pm[2\bar{1}\bar{1}0]$ and $\pm[\bar{2}203]$. The $\pm[2\bar{1}\bar{1}0]$ directions are equal to the a vector of the basal plane, which is the shortest distance between neighbouring metal atoms. These directions are the most commonly observed slip direction of dislocations in hexagonal crystal lattices and were found commonly found by other researchers [9-11] but the observation of $\pm[\bar{2}203]$ Burgers vectors is new.

References

[1] P.C. Cobb, Material & Design 11 (1990) 156.

[2] T. Lundström, Boron and Refractory Borides (1977) 351.

[3] N. Ichinose, Introduction to Fine Ceramics (1987).

[4] A.D. McLeod, J.S. Haggerty and D.R. Sadoway, J. Am. Ceram. Soc. 67 (1984) 705.

[5] J.R. Ramberg, C.F. Wolfe and W.S.

Williams, J. Am. Ceram. Soc. 68 (1985) C-78.

[6] J.R. Ramberg and W.S. Williams, J. Mater. Sic. 22 (1987) 1815.

[7] B. Ralph, University of Wales Review 4 (1988) 29.

[8] N.N. Greenwood, R.V. Parish and P. Thornton, Quarterly Rev. 20 (1966) 441.

[9] S.A. Mersol, C.T. Lynch and F.W. Vahldiek, Anisotropy in Single-Crystal Refractory Compounds (1968) 2.

[10] K. Nakano, T. Imura and S.H. Takeuchi, Japan J. Appl. Phy. 12 (1974) 186.

[11] L. Wang and R.J. Arsenault, Phil. Mag. A-63 (1991) 121.

[12] C.B. Carter and S.L. Sass, J. Am. Ceram. Soc. 64 (1981) 335.

[13] V. Randle and B. Ralph, J. of Mater. Sci. 22 (1987) 2535.

[14] B. Ralph, K.B. Shim, Z. Huda, J. Furley and M.J. Edirisinghe, Mat. Sci. Forum 94-96 (1992) 129.

[15] K.B. Shim, J. Kwiencinski, M.J. Edirisinghe and B. Ralph, Mater. Char. 31 (1993) 39.

[16] E.D. Case, J.R. Smith and O. Hunter, J. Mater. Sci. 15 (1980) 149.

[17] K.T. Faber and A.G. Evans, Acta. Metall. 31 (1983) 565.

[18] H.R. Baumgartner and R.A. Steiger, J. Am. Ceram. Soc. 67 (1984) 207.